An Investigation of Superexchange in Dinuclear Mixed-Valence Ruthenium Complexes

Christopher E. B. Evans,† Mark L. Naklicki,† Ali R. Rezvani,† Christopher A. White,† Veniamin V. Kondratiev,‡ and Robert J. Crutchley*,†

Contribution from the Ottawa-Carleton Chemistry Institute, Carleton University, 1125 Colonel By Drive, Ottawa, Ontario, Canada K1S 5B6, and St. Petersburg University, Universitekaja nab. 7-9, St. Petersburg 199034, Russia

Received July 28, 1998

Abstract: A quantitative study of hole-transfer superexchange in Class II mixed-valence complexes is presented. The free energy of resonance exchange was calculated from metal−metal coupling elements derived from Hush and CNS models and compared to experimental values that were factored from the free energy of comproportionation. The Hush model gave acceptable results for only the most weakly coupled systems while the CNS model gave reasonable predictions throughout the range of coupling studied (valence trapped to nearly delocalized behavior).

Introduction

In a previous study,[1] we reported on the properties of $[\{Ru(NH_3)_5\}_2(\mu\text{-L})]^{3+/4+}$, where L is 2,5-dimethyl-1,4-dicyanamidobenzene, in which the degree of metal−metal coupling was remarkably affected by the nature of the outer coordination sphere. This high sensitivity has application to molecular switching devices,[2] and in addition permits a comprehensive examination of the electronic factors governing superexchange metal−metal coupling. Since that time, we have expanded the family of dinuclear ruthenium dicyd complexes to include not only pentaammine systems,[3] $[\{Ru(NH_3)_5\}_2(\mu\text{-L})]^{4+}$, where L = 2,5-dimethyl- (Me_2dicyd^{2-}), 2,5 dichloro- (Cl_2dicyd^{2-}), 2,3,5,6-tetrachloro- (Cl_4dicyd^{2-}), and unsubtitituted 1,4-dicyanamidobenzene dianion ($dicyd^{2-}$), but also tetraammine systems,[4] $[\{trans\text{-}Ru(NH_3)_4(py)\}_2(\mu\text{-L})]^{4+}$, where py = pyridine and L = Me_2dicyd^{2-}, $dicyd^{2-}$, Cl_2dicyd^{2-}, and Cl_4dicyd^{2-}, and triammine systems,[5] $[\{mer\text{-}Ru(NH_3)_3(bpy)\}_2(\mu\text{-L})]^{4+}$, where bpy = 2,2′-bipyridine and L = Me_2dicyd^{2-}, $dicyd^{2-}$, and Cl_2dicyd^{2-}. Thus, in addition to outer sphere perturbations, inner sphere perturbations of superexchange metal−metal coupling can be explored. The trends in metal−metal coupling that were found for these complexes support the conclusion that the dominant pathway for superexchange occurs via a hole-transfer mechanism.[3−5] A schematic representation hole-transfer superexchange is shown in Figure 1.

In Figure 1, the concerted superexchange event in a mixed-valence complex is represented as sequential electron-transfer events occurring first between the π-HOMO of the bridging ligand and the Ru^{III} (acceptor) dπ orbital and second between the π-HOMO of the bridging ligand and the Ru^{II} (donor) dπ orbital. This mechanism is described as "hole-transfer" because the concerted event is that of an electron hole moving from right to left across the complex. If the metal-to-metal charge transfer (MMCT, often called an intervalence transition, IT, because the metals are of inequivalent oxidation state) was mediated by the ligand's LUMO, the superexchange event would be termed "electron transfer" since the analogous mechanism's sequence of events is that of an electron moving from right to left across the complex (i.e. the sequence of conceptual charge transfers is reversed).

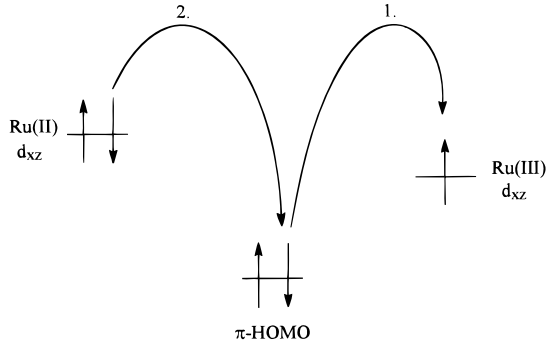

Figure 1. Schematic representation of the hole-transfer superexchange mechanism representing the concerted event as two sequential electron transfers between the bridging ligand's π-HOMO and the ruthenium acceptor and donor d_{xz} orbitals.

Qualitatively, the smaller the energy gap between the ruthenium $d\pi$-orbitals and the HOMO of the bridging ligand, the greater the degree of metal−metal coupling. Spectator ligands on ruthenium and substituents on the bridging ligand perturb the energies of these orbitals according to their electronic properties. Outer sphere perturbations result from donor−acceptor interactions between solvent molecules and ammine ligands. This mechanism has been invoked to explain the solvatochromism of charge-transfer bands in mononuclear ruthenium ammine complexes[6] and the solvent dependent metal−metal coupling in asymmetric dinuclear ruthenium

* Corresponding author.
† Carleton University.
‡ St. Petersburg University.

(1) Naklicki, M. L.; Crutchley, R. J. *J. Am. Chem. Soc*. **1994**, *116*, 6045.
(2) Ward, M. D. *Chem. Soc. Rev.* **1995**, 121
(3) (a) Aquino, M. A. S. Ph.D. Thesis, Carleton University, 1991. (b) Aquino, M. A. S.; Lee, F. L.; Gabe, E. J.; Bensimon, C.; Greedan, J. E.; Crutchley, R. J. *J. Am. Chem. Soc*. **1992**, *114*, 5130. (c) Naklicki, M. L. Ph.D. Thesis, Carleton University, 1995. (d) Naklicki, M. L.; Crutchley, R. J. *Inorg. Chim. Acta* **1994**, *225*, 123.
(4) (a) Rezvani, A. R.; Bensimon, C.; Cromp, B.; Reber, C.; Greedan, J. E.; Kondratiev, V.; Crutchley, R. J. *Inorg. Chem*. **1997**, *36*, 3322. (b) Rezvani, A. R. Ph.D. Thesis, Carleton University, 1995.
(5) Evans, C. E. B.; Yap, G. P. A.; Crutchley, R. J. *Inorg. Chem.* Accepted for publication. Evans, C. E. B. Ph.D. Thesis, Carleton University, 1998.

10.1021/ja982673b CCC: $15.00
Published on Web 12/04/1998

mixed-valence complexes.[7] The stronger the donor−acceptor interaction, the more electron density will be transferred from the ammine to the ruthenium ion. For the complexes of this study, this will raise d-orbital energies and decouple these orbitals from the HOMO of the bridging ligand (Figure 1). Thus, the stronger the donor properties of the solvent, the smaller the magnitude of metal−metal coupling that is experienced by the solvated complex.

In this study we wish to quantitatively evaluate hole transfer superexchange in our mixed-valence systems and our starting point is the model of Hush.[8] This treatment, essentially an application of Mulliken's theories[9] to the specific question of IT bands in mixed-valence complexes, is based upon consideration of the oscillator strength, *f*, of the IT band, and yields the Mulliken−Hush eq 1, by equating theoretical and experimental expressions for *f*.

$$H_{ad} = \frac{2.06 \times 10^{-2}}{r}(\epsilon_{max} \cdot \Delta\nu_{1/2} \cdot E_{IT})^{1/2} \qquad (1)$$

In eq 1, H_{ad} is the donor−acceptor coupling element, r the transition moment length (typically taken as the donor−acceptor separation in Å), and ϵ_{max}, $\Delta\nu_{1/2}$, and E_{IT} are the molar absorptivity ($M^{-1}\cdot cm^{-1}$), bandwidth at half-height (cm^{-1}), and energy at band maximum (cm^{-1}), respectively, of the IT band. In addition, the bandwidth may be predicted by $\Delta\nu_{1/2} = (2310E_{IT})^{1/2}$. Given its success at predicting bandwidths for weakly coupled systems, the model was widely accepted, and believed to be applicable only in the perturbative (i.e. weakly coupled) limit. In 1994, however, Creutz, Newton, and Sutin (CNS) of the Brookhaven National Laboratory revisited the derivation of eq 1, and showed[10] that it can be used to calculate metal−ligand coupling elements for any donor−acceptor system provided overlap may be neglected and the charge-transfer transition dipole moment lies along the donor−acceptor bonding axis. In practice, metal−ligand coupling elements could then be determined from eq 1 by replacing intervalence spectral data with the corresponding metal-to-ligand or ligand-to-metal charge-transfer spectral data.

These facts are central to the most recent model for evaluating metal−metal coupling,[10] which we have coined the CNS model, the main equation of which was derived from second-order wave functions, assuming no direct overlap of the metal orbitals due to their spatial separation. The general equation[11] for the effective (i.e. indirect) coupling of the metal centers is

$$H_{MM'} = \frac{H_{ML}H_{M'L}}{2\Delta E^{eff}_{ML}} + \frac{H_{LM}H_{LM'}}{\Delta E^{eff}_{LM}} \qquad (2)$$

The coupling element $H_{MM'}$ of eq 2 is the effective metal−metal coupling, while the coupling elements in the two terms on the right of eq 2 are associated with metal−ligand interactions of the electron-transfer and hole-transfer pathways, respectively. The denominators are reduced energy gaps between metal and ligand orbitals. The subscript nomenclature may be understood given that the electron-transfer pathway is associated with metal-to-ligand charge transfer (MLCT) bands in the electronic spectrum of the complex, while the hole-transfer pathway is associated with ligand-to-metal (LMCT) bands, as seen in Figure 1.

The CNS approach mimics the superexchange mechanism for which the metal centers couple to each other indirectly via orbitals of the bridging ligand. Often, the energetics of a given system will cause one superexchange mechanism to dominate metal−metal coupling. In such an instance, only the term of eq 2 appropriate to that pathway needs to be considered.[10] For the complexes of this study, only the hole-transfer pathway, and thus the second term of eq 2, needs to be considered. The difference between the terms H_{LM} and $H_{LM'}$ must also be understood. The former reflects ligand−metal interactions for a "normal" LMCT transition, e.g. the event labeled 1 in Figure 1. $H_{LM'}$, on the other hand, is the coupling element for the LMCT event between the ligand and the donor metal center bearing, instantaneously, the charge of the acceptor center.[10] This means that the Ru^{III} center must possess the inner and outer coordination sphere appropriate to a Ru^{II} center. Given that this latter transition is experimentally unobservable, the assumption that $H_{LM} = H_{LM'}$ must be made, introducing a certain inherent error into eq 3, the practical form of eq 2 used in this study.

$$H_{MM'} = \frac{H^2_{LM}}{\Delta E^{eff}_{LM}} \qquad (3)$$

H_{LM} is evaluated with eq 1 and spectroscopic parameters of the LMCT band. The reduced energy gap for the hole-transfer case is given by

$$\Delta E^{eff}_{LM} = \left[0.5\left(\frac{1}{E_{LMCT}} + \frac{1}{E_{LMCT} - E_{IT}}\right)\right]^{-1} \qquad (4)$$

To evaluate the Hush and CNS models of metal−metal coupling, an experimental measure of metal−metal coupling is needed. For a mixed-valence complex, this measure is provided by the free energy of comproportionation, ΔG_c, according to the comproportionation equilibrium,

$$[Ru(II)-Ru(II)] + [Ru(III)-Ru(III)] \overset{K_c}{\rightleftharpoons} 2[Ru(III)-Ru(II)] \qquad (5)$$

that also defines the comproportionation constant, K_c.[12] ΔG_c may be determined electrochemically by using cyclic voltammetry, where the difference between metal centered redox couple potentials, $\Delta E = E^\circ_{M2} - E^\circ_{M1}$,

$$[Ru(II)-Ru(II)] \overset{E^\circ_{M1}}{\rightleftharpoons} [Ru(III)-Ru(II)] \overset{E^\circ_{M2}}{\rightleftharpoons} [Ru(III)-Ru(III)] \qquad (6)$$

can be related to the free energy of comproportionation via the Nernst equation.

The magnitude of K_c is determined by the sum of all energetic factors relating to the stability of the reactant and product complexes. According to Sutton and Taube,[13] four distinct

(6) (a) Curtis, J. C.; Sullivan, B. P.; Meyer, T. J. *Inorg. Chem.* **1983**, *22*, 224. (b) Neyhart, G. A.; Timpson, C. J.; Bates, W. D.; Meyer, T. J. *J. Am. Chem. Soc*. **1996**, *118*, 3730. (c) Neyhart, G. A.; Hupp, J. T.; Curtis, J. C.; Timpson, C. J.; Meyer, T. J. *J. Am. Chem. Soc*. **1996**, *118*, 3724.

(7) Chang, J. P.; Fung, E. Y.; Curtis, J. C. *Inorg. Chem*. **1986**, *25*, 4233.

(8) Hush, N. S. *Prog. Inorg. Chem.*, **1967**, *8*, 391.

(9) Mulliken, R. S.; Person, W. B. *Molecular Complexes*; John Wiley & Sons: New York, 1969.

(10) Creutz, C.; Newton, M. D.; Sutin, N. *J. Photochem. Photobiol. A: Chem.* **1994**, *82*, 47.

(11) It should be noted that eq 2 differs from the corresponding equation in ref 10 in that the MLCT term possesses a factor of 1/2 while the LMCT term does not. The MLCT states involve two degenerate zero-order configurations and so the metal−ligand coupling terms require a correction of $1/\sqrt{2}$ each. For each LMCT state, only one configuration is possible and so no correction for degeneracy is necessary. We are grateful to Norman Sutin for pointing out to us that eq 2 is the correct form to use when both Ru(II) MLCT and Ru(III) LMCT states contribute to the superexchange.

(12) Creutz, C. *Prog. Inorg. Chem.* **1983**, *30*, 1.

(13) Sutton, J. E.; Sutton, P. M.; Taube, H. *Inorg. Chem.* **1979**, *18*, 1017.

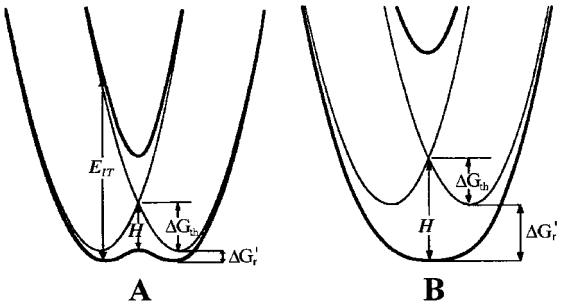

Figure 2. Potential energy curves for Class I (light line in both A and B), Class II (A), and Class III (B) symmetric mixed valence complexes.

factors contribute to the magnitude of ΔG_c:

$$\Delta G_c = \Delta G_s + \Delta G_e + \Delta G_i + \Delta G_r \quad (7)$$

In eq 7, ΔG_s reflects the statistical distribution of the comproportionation equilibrium, ΔG_e accounts for the electrostatic repulsion of the two like-charged metal centers, ΔG_i is an inductive factor dealing with competitive coordination of the bridging ligand by the metal ions, and ΔG_r is the free energy of resonance exchange—the only component of ΔG_c which represents "actual" metal−metal coupling. Recently, Sutin[14] has pointed out the need for another term in cases where antiferromagnetic exchange significantly stabilizes one of the reactants of eq 5. This term, ΔG_{ex}, is then a fifth contributing factor to the magnitude of ΔG_c,

$$\Delta G_c = \Delta G_s + \Delta G_e + \Delta G_i + \Delta G_r + \Delta G_{ex} \quad (8)$$

Unlike the other four terms, which all favor the mixed-valence product of eq 3, ΔG_{ex} measures a stabilizing influence upon a reactant complex, and thus is of opposite sign to the remaining terms of eq 8.

In systems where superexchange occurs via the electron-transfer pathway, energetic mismatch of the ligand π-LUMO and the Ru(III) πd orbitals should lead to a small or insignificant magnitude of ΔG_{ex}. In hole-transfer systems, however, the magnitude of ΔG_{ex} may be such that ignoring this term leads to misleadingly low estimates of resonance exchange.

An experimental value for the free energy of resonance exchange ΔG_r therefore requires that the other terms in eq 8 be quantitatively evaluated. As we will show, the properties of the complexes of this study make this determination uniquely possible.

A mixed-valence complex will fall into one of three categories, as proposed by Robin and Day,[15] depending upon the degree of coupling between the metal centers. Completely valence trapped complexes (no coupling between the metal centers) are termed Class I while complexes in which the valence electrons are fully delocalized (very strong coupling between the metal centers) are termed Class III. All complexes whose behavior falls between these extremes constitute Class II. The potential energy curves in Figure 2 illustrate the Class I, Class II, and Class III cases. E_{IT}, H (H_{ad} or $H_{MM'}$) and ΔG_{th} are the intervalence band energy, metal−metal coupling element and the thermal electron-transfer barrier, respectively. The free energy of comproportionation ΔG_c results from the formation of two mixed-valence complexes (eq 5). To be consistent with our theoretical analysis, we must consider the free energy of comproportionation per mixed-valence complex or $\Delta G_c' = 0.5\Delta G_c$. By analogy, we define the free energy of resonance exchange per mixed valence complex as $\Delta G_r' = 0.5\Delta G_r$. In the weak coupling case for symmetric systems, it has been shown[16] that

$$\Delta G_r' = H^2/E_{IT} \quad (9)$$

whereas, for the strongly coupled Class III systems (Figure 2B),

$$\Delta G_r' = H - \Delta G_{th} \quad (10)$$

ΔG_{th} for ruthenium ammine complexes varies from 2000 to 3000 cm^{-1}.[16] As we will later show, most of the complexes of this study have metal−metal coupling elements that are smaller than this range. Accordingly, the intermediate coupling case in Figure 2A provides the best description for the majority of the complexes of this study and our theoretical value of the free energy of resonance exchange will be derived from eq 9.[17]

Experimental Section

The syntheses of $[\{Ru(NH_3)_5\}_2(\mu\text{-L})][PF_6]_4$[3] and $[\{trans\text{-}Ru(NH_3)_4(py)\}_2(\mu\text{-L})][PF_6]_4$,[4] where L = Me_2dicyd^{2-}, $dicyd^{2-}$, Cl_2dicyd^{2-}, and Cl_4dicyd^{2-} and py = pyridine, and of $[\{mer\text{-}Ru(NH_3)_3(bpy)\}_2(\mu\text{-L})][ClO_4]_4$,[5] where L = Me_2dicyd^{2-}, $dicyd^{2-}$, and Cl_2dicyd^{2-} and bpy = 2,2′-bipyridine, have all been previously reported. Electronic absorption spectroscopy was performed on a Varian Cary 5 UV−Vis−NIR spectrophotometer at ambient temperatures with use of quartz cells of either 1.000 (pentaammine and tetraammine complexes) or 0.200 cm (triammine complexes) path length from Hellma (Canada) Limited.[4,5] Cyclic voltammetry was performed with a BAS CV-27 voltammograph and three-electrode systems consisting of platinum-disk working, platinum-wire counter, and silver-wire quasi-reference electrodes, on solutions, at 25 °C, containing complex and 0.1 M tetrabutylammonium hexafluorophosphate electrolyte. The electrochemistry internal reference, ferrocene (J. T. Baker), was purified by sublimation and tetrabutylammonium hexafluorophosphate (TBAH) was recrystallized twice from 2:1 ethanol:water and vacuum-dried overnight at 110 °C. Spectroelectrochemistry of the tetraammine complexes was performed in an H-cell,[18] while an OTTLE cell based upon the design of Hartl[5,19] was used for the spectroelectrochemical measurements of the pentaammine and triammine complexes. Organic solvents used for spectroscopy or electrochemistry were Anachemia *Accusolv* grade unless otherwise noted, and were distilled in glass at reduced pressure and stored under argon. With the exception of acetone (AC), all solvents were dried with an appropriate reagent. Acetonitrile (AN) was distilled in the presence of phosphorus pentoxide, dimethyl sulfoxide (DMSO) and nitromethane (NM) (HPLC grade, 96+%, Sigma) were dried overnight with, and distilled in the presence of, aluminum oxide (neutral, chromatography grade, Woelm) activated by heating to 300 °C for several hours in a muffle furnace.

Results and Discussion

The visible−NIR spectra of all [III,III] complexes of this study are dominated by an intense band assigned as an LMCT transition.[3,20] Upon electrochemical reduction of the complex to the mixed-valence state, this LMCT band loses intensity while a low-energy shoulder, assigned as an IT band, grows in.[3]

(14) Norman Sutin, personal communication.

(15) Robin, M. B.; Day, P. *Adv. Inorg. Chem. Radiochem.* **1967**, *10*, 247.

(16) Richardson, D. E.; Taube, H. *Coord. Chem. Rev.* **1984**, *60*, 107.

(17) In previous studies (see ref 4), we plotted experimental $\Delta G_r'$ against the CNS model calculated $H_{MM'}$. While the resulting linear plots possessed excellent correlation coefficients, eq 9 shows that this will occur only when $H_{MM'}/E_{IT}$ is constant. It is not obvious why this relationship should hold for all Class II systems and so the result may be fortuitous.

(18) Brewer, K. J.; Calvin, M.; Lummpkin, R. S.; Otvos, J. W.; Spreer, L. O. *Inorg. Chem.* **1989,** *28*, 4446.

(19) Krejcik, M.; Danek, M.; Hartl, F. *J. Electroanal. Chem.* **1991**, *317*, 179.

(20) (a) Crutchley, R. J.; Naklicki, M. L. *Inorg. Chem.* **1989**, *28*, 1955. (b) Evans, C. E. B.; Ducharme, D.; Naklicki, M. L.; Crutchley, R. J. *Inorg. Chem.*, **1995**, *34*, 1350.

Table 1. Electronic Absorption Data for the LMCT and IT Bands of the Complexes $[\{Ru(NH_3)_5\}_2(\mu\text{-L})]^{4+/3+}$, Respectively, as a Function of Ligand and Solvent[a]

		LMCT			IT		
L	solvent[b]	f' [c]	ϵ_{max}	E_{LMCT}	ϵ_{max}	E_{IT}	$\nu_{1/2}$
Me_2dicyd^{2-}	AN (14.1)	0.342	6.46×10^4	8920	1.98×10^4	7100	2430
Me_2dicyd^{2-}	AC (17.0)	0.275	4.27×10^4	8940	1.64×10^4	6930	2350
Me_2dicyd^{2-}	DMSO (29.8)	0.186	1.58×10^4	9890	9.26×10^3	6890	3760
$dicyd^{2-}$	NM (2.7)	0.338	6.31×10^4	9030	2.06×10^4	6980	2430
$dicyd^{2-}$	AN (14.1)	0.305	4.57×10^4	9140	2.00×10^4	6890	2760
$dicyd^{2-}$	AC (17.0)	0.239	2.95×10^4	9200	1.62×10^4	6750	2760
$dicyd^{2-}$	DMSO (29.8)	0.176	1.41×10^4	11060	7.59×10^3	7500	4250
Cl_2dicyd^{2-}	AN (14.1)	0.234	2.19×10^4	9940	1.58×10^4	6910	3390
Cl_2dicyd^{2-}	AC (17.0)	0.200	1.66×10^4	10380	1.06×10^4	7080	3790
Cl_2dicyd^{2-}	DMSO (29.8)	0.138	1.15×10^4	12640	5.88×10^3	7950	5720
Cl_4dicyd^{2-}	AN (14.1)	0.150	1.41×10^4	12000	7.78×10^3	7320	3890

[a] Data in units of cm^{-1} except ϵ_{max}, which has units of $L \cdot mol^{-1} \cdot cm^{-1}$. [b] Solvent donor number in parentheses. [c] f' has been normalized for a single Ru−NCN chromophore.

Table 2. Electronic Absorption Data for the LMCT and IT Bands of the Complexes $[\{trans\text{-}Ru(NH_3)_4(py)\}_2(\mu\text{-L})]^{4+/3+}$, Respectively, as a Function of Ligand and Solvent[a]

		LMCT			IT		
L	solvent[b]	f' [c]	ϵ_{max}	E_{LMCT}	ϵ_{max}	E_{IT}	$\nu_{1/2}$
Me_2dicyd^{2-}	NM (2.7)	0.455	7.45×10^4	8890	1.69×10^4	7390	2200
Me_2dicyd^{2-}	AN (14.1)	0.421	7.58×10^4	8880	2.14×10^4	7480	1920
Me_2dicyd^{2-}	DMSO (29.8)	0.220	4.21×10^4	8520	1.85×10^4	6540	2380
$dicyd^{2-}$	NM (2.7)	0.404	6.95×10^4	8890	1.57×10^4	7340	2000
$dicyd^{2-}$	AN (14.1)	0.386	7.54×10^4	8600	2.41×10^4	7230	2090
$dicyd^{2-}$	DMSO (29.8)	0.284	4.11×10^4	8510	2.24×10^4	6460	2830
Cl_2dicyd^{2-}	NM (2.7)	0.328	6.33×10^4	8460	2.45×10^4	6580	2240
Cl_2dicyd^{2-}	AN (14.1)	0.300	4.24×10^4	8510	2.13×10^4	6690	2700
Cl_2dicyd^{2-}	DMSO (29.8)	0.200	1.73×10^4	9670	1.00×10^4	6910	3750
Cl_4dicyd^{2-}	NM (2.7)	0.301	4.16×10^4	8810	2.13×10^4	6260	2980
Cl_4dicyd^{2-}	AN (14.1)	0.289	2.63×10^4	9350	1.70×10^4	6580	3350
Cl_4dicyd^{2-}	DMSO (29.8)	0.173	1.36×10^4	11890	6.09×10^3	7670	4530

[a] Data in units of cm^{-1} except ϵ_{max}, which has units of $L \cdot mol^{-1} \cdot cm^{-1}$. [b] Solvent donor number in parentheses. [c] f' has been normalized for a single Ru−NCN chromophore.

Table 3. Electronic Absorption Data for the LMCT and IT Bands of the Complexes $[\{mer\text{-}Ru(NH_3)_3(bpy)\}_2(\mu\text{-L})]^{4+/3+}$, Respectively, as a Function of Ligand and Solvent[a]

		LMCT			IT		
L	solvent[b]	f' [c]	ϵ_{max}	E_{LMCT}	ϵ_{max}	E_{IT}	$\nu_{1/2}$
Me_2dicyd^{2-}	AN (14.1)	0.414	5.53×10^4	9510	1.18×10^4	7970	1760
$dicyd^{2-}$	AN (14.1)	0.447	7.05×10^4	8940	1.82×10^4	7550	1700
$dicyd^{2-}$	DMSO (29.8)	0.399	7.40×10^4	8120	2.26×10^4	6670	2340
Cl_2dicyd^{2-}	NM (2.7)	0.433	7.50×10^4	8510	2.40×10^4	7000	2290
Cl_2dicyd^{2-}	AN (14.1)	0.407	7.60×10^4	8350	2.80×10^4	6910	2440
Cl_2dicyd^{2-}	AC (17.0)	0.405	8.11×10^4	8250	3.11×10^4	6780	2140
Cl_2dicyd^{2-}	DMSO (29.8)	0.283	3.79×10^4	8320	2.53×10^4	6400	3440

[a] Data in units of cm^{-1} except ϵ_{max}, which has units of $L \cdot mol^{-1} \cdot cm^{-1}$. [b] Solvent donor number in parentheses. [c] f' has been normalized for a single Ru−NCN chromophore.

Determination of the oscillator strength of the LMCT band[20b] and deconvolution of the IT band from the band envelope of the mixed-valence complex have been described elsewhere.[3d] Spectral parameters of the LMCT and IT bands of the complexes in various solvents have been placed in Tables 1−3. In Figure 3, representative spectra of the low-energy LMCT band of $[\{mer\text{-}Ru(NH_3)_3(bpy)\}_2(\mu\text{-dicyd})]^{4+}$ and $[\{Ru(NH_3)_5\}_2(\mu\text{-dicyd})]^{4+}$ are shown as a function of solvent. The solvent dependence of the pentaammine complexes' LMCT band (Figure 3B) is greater than that for the corresponding triammine complexes, and may be understood in terms of the number of solvent−ammine donor−acceptor interactions, which weaken the Ru−cyanamide bond, and the energy diagram of Figure 1, where increasing donating ability of the solvent raises the energy of the metal πd orbitals, shifting the LMCT to higher energy. The weakening of the Ru−cyanamide bond is paralleled by a decrease in LMCT band oscillator strength. This is in accord with the predictions of the CNS model that uses eq 1 to calculate metal−ligand coupling elements. For the triammine complex in Figure 3A, a steady decrease in LMCT oscillator strength with increasing donor number of the solvent is not apparent and we suggest that this is a consequence of the increased covalency of the Ru−cyanamide bond.

In Figure 4, the spectra of [III,III] and [III,II] complexes, $[\{mer\text{-}Ru(NH_3)_3(bpy)\}_2(\mu\text{-dicyd})]^{4+,3+}$ and $[\{Ru(NH_3)_5\}_2(\mu\text{-dicyd})]^{4+,3+}$ in acetonitrile, are shown. The [II, II] complexes absorb weakly in the visible−NIR range and so the difference between the spectra of [III, III] and [III, II] complexes is due to the presence of an IT band and the loss of a Ru(III)−cyanamide LMCT chromophore upon reduction of the [III, III] complex. It is interesting to contrast the broad, intense IT band of the more weakly coupled pentaammine complex, Figure 4B, with the narrower and less intense IT band for the more strongly coupled triammine complex, Figure 4A. The change in the

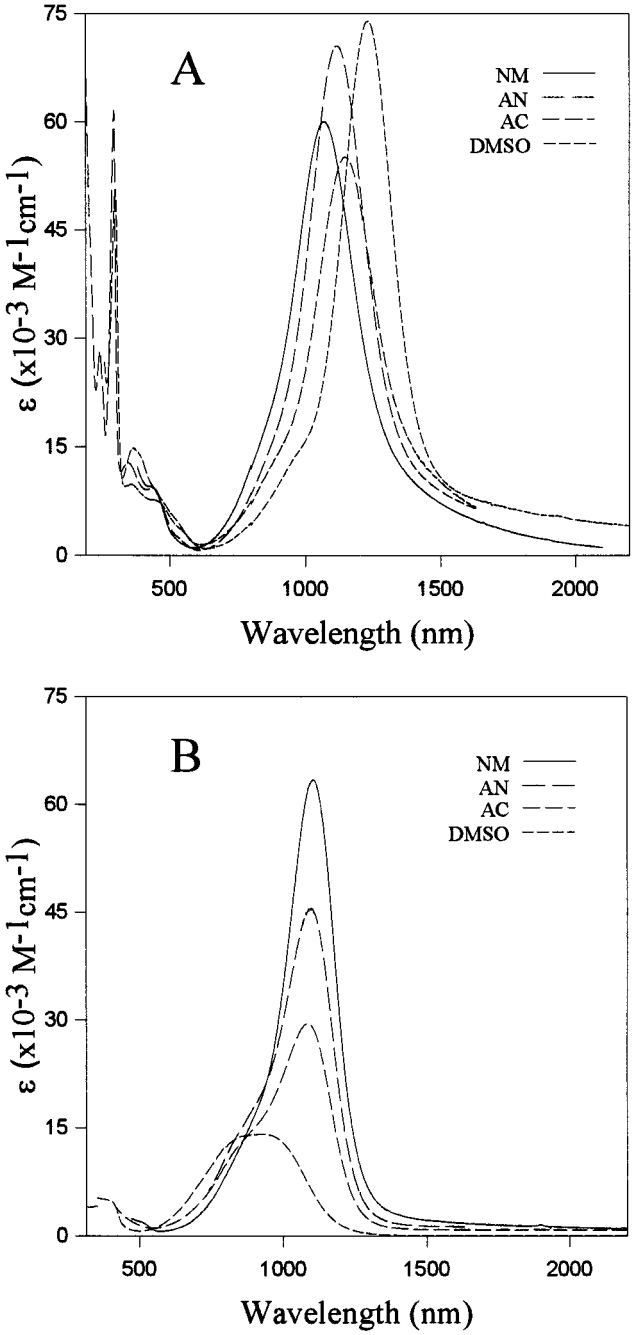

Figure 3. Solvent dependence of the LMCT band of (A) [{*mer*-Ru(NH$_3$)$_3$(bpy)}$_2$(μ-dicyd)]$^{4+}$ and (B) [{Ru(NH$_3$)$_5$}$_2$(μ-dicyd)]$^{4+}$.

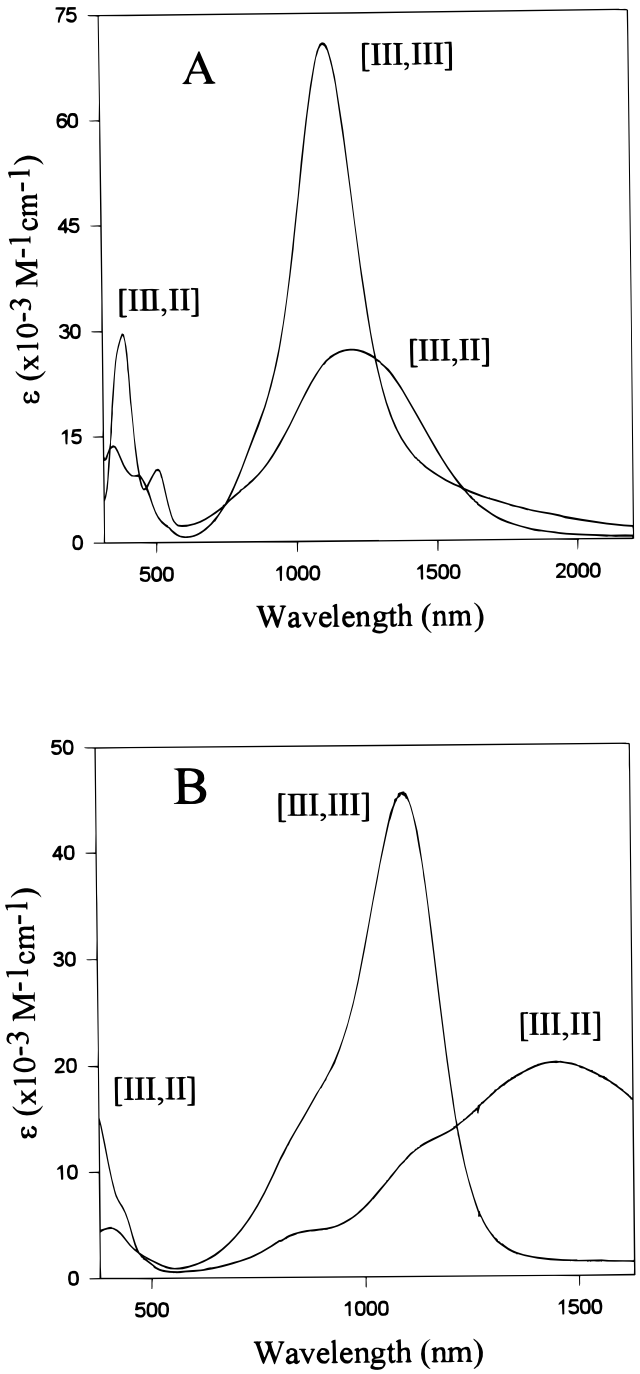

Figure 4. Visible and NIR spectra of the [III, III] and [III, II] complexes of (A) [{*mer*-Ru(NH$_3$)$_3$(bpy)}$_2$(μ-dicyd)]$^{4+/3+}$ and (B) [{Ru(NH$_3$)$_5$}$_2$(μ-dicyd)]$^{4+/3+}$, in acetonitrile showing LMCT and IT bands.

oscillator strength of the IT bands is not in accord with the predictions of the Hush model (eq 1) and may be due to the inappropriateness of using the metal-to-metal distance to approximate the transition dipole moment length. This error is expected to increase as the odd electron of the mixed valence species becomes increasingly delocalized.

The cyclic voltammetry of the complexes of this study has already been discussed.[3−5] For the purposes of this study, we are interested in the separation between the two Ru(III/II) couples as a measure of the comproportionation constant K_c. The latter value together with the free energy of comproportionation ΔG_c can be found in Tables 5−7.

Understanding the solvent dependence of the free energy of comproportionation requires that one consider the various terms of eq 8. The value of ΔG_s may be calculated by recognizing that it stems directly from the statistical distribution of the comproportionation equilibrium, which implies $K_c = 4$ for a symmetrical system, and which relates to $\Delta G_s \approx 290$ cm^{-1}.[21] ΔG_e may be evaluated according to eq 11, which assumes the

Table 4. Solvent Dependence of ΔG_e and ΔG_{ne}

solvent	ϵ[a]	ΔG_e (cm^{-1})[b]	ΔG_{ne} (cm^{-1})[c]
nitromethane	35.87	250	660
acetonitrile	35.94	240	650
acetone	20.56	430	840
dimethyl sulfoxide	46.45	190	600
water	78.36	110	520

[a] Data at 25 °C except NM at 30 °C; see ref 22b. [b] Calculated by using eq 11 assuming $R_{12} = 13.1$ Å. [c] $\Delta G_{ne} = 520 + [\Delta G_e(\text{solvent}) - \Delta G_e(\text{water})]$.

Table 5. Free Energy of Comproportionation Data[a] for the Complexes $[\{Ru(NH_3)_5\}_2(\mu\text{-L})]^{3+}$ as a Function of Ligand and Solvent

L	solvent[b]	K_c[c]	ΔG_c	$\Delta G_c - \Delta G_{ne}$[d]	ΔG_{ex}[e]	ΔG_r[f]
Me_2dicyd^{2-}	AN (14.1)	5.6×10^5	2740	2090	330	2420
Me_2dicyd^{2-}	AC (17.0)	3.1×10^5	2620	1780	320	2100
Me_2dicyd^{2-}	DMSO (29.8)	2.2×10^3	1600	1000	210	1210
$dicyd^{2-}$	NM (2.7)	2.0×10^5	2520	1860	360	2220
$dicyd^{2-}$	AN (14.1)	6.9×10^4	2310	1660	310	1970
$dicyd^{2-}$	AC (17.0)	1.4×10^4	1980	1140	290	1430
$dicyd^{2-}$	DMSO (29.8)	6.7×10^2	1350	750	190	940
Cl_2dicyd^{2-}	AN (14.1)	3.9×10^3	1710	1060	230	1290
Cl_2dicyd^{2-}	AC (17.0)	2.1×10^3	1580	740	210	950
Cl_2dicyd^{2-}	DMSO (29.8)	1.6×10^2	1050	450	160	610
Cl_4dicyd^{2-}	AN (14.1)	3.3×10^2	1200	550	180	730

[a] All data in cm^{-1} except K_c, which is unitless. [b] Solvent donor number in parentheses. [c] From the difference in Ru(III)/(II) reduction couples ΔE and calculated by $K_c = \exp(16.91\Delta E)$. [d] ΔG_{ne} values are in Table 4. [e] ΔG_{ex} or $-J$ (antiferromagnetic exchange) values are in ref 24. [f] $\Delta G_r = \Delta G_c - \Delta G_{ne} + \Delta G_{ex}$.

Table 6. Free Energy of Comproportionation Data[a] for the Complexes $[\{trans\text{-}Ru(NH_3)_4(py)\}_2(\mu\text{-L})]^{3+}$ as a Function of Ligand and Solvent

L	solvent[b]	K_c[c]	ΔG_c	$\Delta G_c - \Delta G_{ne}$[d]	ΔG_{ex}[e]	ΔG_r[g]
Me_2dicyd^{2-}	NM (2.7)	2.2×10^6	3020	2360	*f*	
Me_2dicyd^{2-}	AN (14.1)	5.2×10^6	3200	2550	360	2910
Me_2dicyd^{2-}	DMSO (29.8)	5.2×10^4	2250	1650	310	1960
$dicyd^{2-}$	NM (2.7)	1.4×10^6	3070	2410	*f*	
$dicyd^{2-}$	AN (14.1)	1.2×10^6	2900	2250	340	2590
$dicyd^{2-}$	DMSO (29.8)	7.8×10^3	1860	1260	240	1500
Cl_2dicyd^{2-}	NM (2.7)	1.1×10^5	2400	1740	*f*	
Cl_2dicyd^{2-}	AN (14.1)	2.7×10^4	2110	1460	230	1690
Cl_2dicyd^{2-}	DMSO (29.8)	3.4×10^2	1210	610	190	800
Cl_4dicyd^{2-}	NM (2.7)	3.9×10^3	1710	1050	*f*	
Cl_4dicyd^{2-}	AN (14.1)	7.2×10^2	1360	710	200	910
Cl_4dicyd^{2-}	DMSO (29.8)	1.5×10^2	1030	430	160	590

[a] All data in cm^{-1} except K_c, which is unitless. [b] Solvent donor number in parentheses. [c] From the difference in Ru(III)/(II) reduction couples ΔE and calculated by $K_c = \exp(16.91\Delta E)$. [d] ΔG_{ne} values are in Table 4. [e] ΔG_{ex} or $-J$ (antiferromagnetic exchange) values were calculated from magnetic moment data in ref 4b and eq 9 in ref 24. [f] Not determined. [g] $\Delta G_r = \Delta G_c - \Delta G_{ne} + \Delta G_{ex}$.

Table 7. Free Energy of Comproportionation Data[a] for the Complexes $[\{mer\text{-}Ru(NH_3)_3(bpy)\}_2(\mu\text{-L})]^{3+}$ as a Function of Ligand and Solvent

L	solvent[b]	K_c[c]	ΔG_c	$\Delta G_c - \Delta G_{ne}$[d]	ΔG_{ex}[e]	ΔG_r[g]
Me_2dicyd^{2-}	AN (14.1)	1.3×10^7	3400	2750	*f*	
$dicyd^{2-}$	AN (14.1)	9.3×10^6	3320	2670	*f*	
$dicyd^{2-}$	DMSO (29.8)	2.1×10^5	2540	1940	*f*	
Cl_2dicyd^{2-}	NM (2.7)	7.7×10^5	2810	2150	*f*	
Cl_2dicyd^{2-}	AN (14.1)	3.5×10^5	2650	2000	310	2310
Cl_2dicyd^{2-}	AC (17.0)	3.1×10^5	2620	1780	*f*	
Cl_2dicyd^{2-}	DMSO (29.8)	3.0×10^3	1660	1060	240[h]	1300

[a] All data in cm^{-1} except K_c, which is unitless. [b] Solvent donor number in parentheses. [c] From the difference in Ru(III)/(II) reduction couples ΔE and calculated by $K_c = \exp(16.91\Delta E)$. [d] ΔG_{ne} values are in Table 4. [e] ΔG_{ex} or $-J$ (antiferromagnetic exchange) values were calculated from magnetic moment data in ref 5b and eq 9 in ref 24. [f] Not determined. [g] $\Delta G_r = \Delta G_c - \Delta G_{ne} + \Delta G_{ex}$. [h] μ_{eff}/Ru(III) = 1.1 μ_B at room temperature.

medium in which the ionic metal centers are found can be treated as a dielectric continuum, and that there is a unit difference in ionic charge between the two centers.[22]

$$\Delta G_e = \frac{1}{4\pi\epsilon\epsilon_o R_{12}} \tag{11}$$

Here R_{12} represents the separation of the metal centers, ϵ the solvent's static dielectric, and ϵ_o the permittivity of free space. A value for R_{12} of 13.1 Å, that found in the crystal structures of both $[\{Ru(NH_3)_5\}_2(\mu\text{-dicyd})][OTs]_4$2b and $[\{mer\text{-}Ru(NH_3)_3(bpy)\}_2(\mu\text{-dicyd})][ClO_4]_4$,[5] has been chosen as appropriate for describing the solvated complexes. Estimates of ΔG_e with eq 11 have been placed in Table 4. The values so determined must be acknowledged to be approximate insofar as the assumption of dielectric continuum is unlikely to be rigorously true and that significant coupling within the complex will tend to delocalize the metals' charges, reducing R_{12} significantly.

The antiferromagnetic exchange term ΔG_{ex} may be estimated from room-temperature magnetic moments (Evans' method NMR experiments)[23] and the Van Vleck expression for magnetic susceptibility.[24] Comprehensive estimates of ΔG_{ex} (or one-half the separation between singlet ground and triplet excited states) are available for the pentaammine complexes and to a lesser extent the tetraammine complexes. For the triammine complexes, autoreduction to the mixed-valence complex and the solubility of the complexes limited the application of the Evans' method to $[\{mer\text{-}Ru(NH_3)_3(bpy)\}_2(\mu\text{-}Cl_2dicyd)][ClO_4]_4$ in acetonitrile and DMSO solutions.

ΔG_s and ΔG_e will contribute significantly to ΔG_c only in very weakly coupled complexes. For example, $[\{Ru(NH_3)_5\}_2(\mu\text{-}Cl_4dicyd)]^{3+}$ in aqueous solution (the most weakly coupled complex in the most decoupling solvent)[3d] was found to have $K_c = 13$ or $\Delta G_c = 520$ cm^{-1}. The contributions of ΔG_s (290 cm^{-1}) and ΔG_e (110 cm^{-1}, Table 4) account for roughly 75% of ΔG_c in this instance. In addition, because ΔG_r and ΔG_{ex} are expected to be very small in the weak coupling case, the inductive term, ΔG_i, is suggested to contribute the remaining 120 cm^{-1}. As mentioned in the Introduction, ΔG_i is an inductive factor dealing with competitive coordination of the bridging ligand by the metal ions. For the complexes of this study, we make the approximation that ΔG_i is constant, because the electronic properties of the bridging ligand and metal ions are only perturbed by substituents and spectator ligands, respectively. Thus, $\Delta G_c = 520$ cm^{-1} for the complex $[\{Ru(NH_3)_5\}_2(\mu\text{-}Cl_4dicyd)]^{3+}$ in aqueous solution provides a reasonable estimate of the nonexchange contributions to ΔG_c, i.e. $\Delta G_{ne} = \Delta G_s + \Delta G_e + \Delta G_i$, for all the complexes of this study in aqueous solution. The values of ΔG_{ne} in other solvents are obtained by adding the absolute difference in ΔG_e between aqueous and aprotic solvent to 520 cm^{-1}. These values have been tabulated in Table 4.

To test the predictive abilities of the Hush and CNS models, the resonance exchange free energies predicted from optical properties with eqs 9 and 1 (Hush) and eqs 9 and 3 (CNS) will be compared with those obtained electrochemically using eqs 5−8. Data for the various terms of both models have been placed in Tables 8−10. For the Hush treatment with eq 1, *r* was chosen to be 13.1 Å, the metal−metal separation determined via crystallography. Figure 5 shows the resultant plot of $\Delta G_r'$ vs

(21) Salaymeh, F.; Berhane, S.; Yusof, R.; de la Rosa, R.; Fung, E. Y.; Matamoros, R.; Lau, K. W.; Zheng, Q.; Kober, E. M.; Curtis, J. C. *Inorg. Chem.* **1993**, *32*, 3895.

(22) (a) Ferrere, S.; Elliott, C. M. *Inorg. Chem.* **1995**, *35*, 5818. (b) Riddick, J. A.; Bunger, W. B.; Sakano, T. K. *Techniques of Chemistry, Vol. II, Organic Solvents: Physical Properties and Methods of Purification*, 4th ed.; Wiley-Interscience: New York, 1986.

(23) (a) Evans, D. F. *J. Chem. Soc.* **1959**, 2003. (b) Phillips, W. D.; Poe, M. *Methods Enzymol.* **1972**, *24*, 304.

(24) Naklicki, M. L.; White, C. A.; Plante, L. L.; Evans, C. E. B.; 25. Crutchley, R. J. *Inorg. Chem.* **1998**, *37*, 1880.

Table 8. Hush Model Predicted Bandwidths and Metal−Metal Coupling Elements, CNS Model Metal−Ligand and Metal−Metal Coupling Elements, and Reduced Metal−Ligand Energy Differences for the Complexes $[\{Ru(NH_3)_5\}_2(\mu\text{-L})]^{3+}$ as a Function of Ligand and Solvent. Experimental Estimates of IT Bandwidths and Free Energies of Resonance Exchange Are Provided for Comparison[a]

		exptl	Hush model		CNS model			exptl
L	solvent	$\Delta\nu_{1/2}$	$\Delta\nu_{1/2}$[b]	H_{ad}	H_{LM}[c]	ΔE_{LM}[d]	$H_{MM'}$[e]	$\Delta G_r'$[f]
Me_2dicyd^{2-}	AN	2430	4050	930	2570	3020	2190	1210
Me_2dicyd^{2-}	AC	2350	4000	820	2310	3280	1630	1050
Me_2dicyd^{2-}	DMSO	3760	3990	780	2000	4600	870	600
$dicyd^{2-}$	NM	2430	4020	940	2570	3340	1980	1110
$dicyd^{2-}$	AN	2760	3990	980	2460	3610	1680	990
$dicyd^{2-}$	AC	2760	3950	870	2180	3870	1230	710
$dicyd^{2-}$	DMSO	4250	4160	780	2050	5390	780	470
Cl_2dicyd^{2-}	AN	3390	4000	960	2250	4640	1090	650
Cl_2dicyd^{2-}	AC	3790	4040	850	2120	5010	900	470
Cl_2dicyd^{2-}	DMSO	5720	4290	820	1940	6840	550	310
Cl_4dicyd^{2-}	AN	3890	4110	750	2180	6730	710	360

[a] All data in cm^{-1}. [b] Hush predicted bandwidths calculated according to $\Delta\nu_{1/2}(\text{Hush}) = (2910\nu_{max})^{1/2}$ cm^{-1}. [c] Calculated according to eqs 12 and 13. [d] Calculated according to eq 4. [e] Calculated according to eq 3. [f] $\Delta G_r' = 0.5(\Delta G_r)$ in Table 5.

Table 9. Hush Model Predicted Bandwidths and Metal−Metal Coupling Elements, CNS Model Metal−Ligand and Metal−Metal Coupling Elements, and Reduced Metal−Ligand Energy Differences for the Complexes $[\{trans\text{-}Ru(NH_3)_4(py)\}_2(\mu\text{-L})]^{3+}$ as a Function of Ligand and Solvent. Experimental Estimates of IT Bandwidths and Free Energies of Resonance Exchange Are Provided for Comparison[a]

		exptl	Hush model		CNS model			exptl
L	solvent	$\Delta\nu_{1/2}$	$\Delta\nu_{1/2}$[b]	H_{ad}	H_{LM}[c]	ΔE_{LM}[d]	$H_{MM'}$[e]	$\Delta G_r'$[f]
Me_2dicyd^{2-}	NM	2200	4130	830	2960	2570	3410	
Me_2dicyd^{2-}	AN	1920	4160	880	2850	2420	3360	1450
Me_2dicyd^{2-}	DMSO	2380	3890	850	2020	3210	1270	980
$dicyd^{2-}$	NM	2000	4120	760	2790	2640	2950	
$dicyd^{2-}$	AN	2090	4090	960	2690	2360	3070	1300
$dicyd^{2-}$	DMSO	2830	3860	1010	2280	3300	1580	750
Cl_2dicyd^{2-}	NM	2240	3900	950	2450	3080	1950	
Cl_2dicyd^{2-}	AN	2700	3930	980	2350	3000	1840	840
Cl_2dicyd^{2-}	DMSO	3750	4000	810	2050	4290	980	400
Cl_4dicyd^{2-}	NM	2980	3800	1000	2400	3960	1450	
Cl_4dicyd^{2-}	AN	3350	3900	970	2420	4270	1370	560
Cl_4dicyd^{2-}	DMSO	4530	4210	730	2110	6230	710	290

[a] All data in cm^{-1}. [b] Hush predicted bandwidths calculated according to $\Delta\nu_{1/2}(\text{Hush}) = (2910\nu_{max})^{1/2}$ cm^{-1}. [c] Calculated according to eqs 12 and 13. [d] Calculated according to eq 4. [e] Calculated according to eq 3. [f] $\Delta G_r' = 0.5(\Delta G_r)$ in Table 6.

H_{ad}^2/E_{IT} for the pentaammine complexes (Table 8). The lack of significant correlation between these two terms is indicative of the Hush model's inappropriateness for complexes as strongly coupled as the ones of this study. In particular, the Hush model predicts only a modest range of $\Delta G_r'$ compared to that experimentally observed. Furthermore, examination of the data in Table 8 shows that while the Hush model predicts $\Delta\nu_{1/2}$ reasonably well for the more weakly coupled complexes ($[\{Ru(NH_3)_5\}_2(\mu\text{-}Cl_4dicyd)]^{3+}$ and $[\{Ru(NH_3)_5\}_2(\mu\text{-}Cl_2dicyd)]^{3+}$) in DMSO solution, as the metal centers become more strongly coupled, experimental $\Delta\nu_{1/2}$ values are significantly less than their estimated counterparts with the error increasing as coupling increases. IT bandwidth is often used as a benchmark for the degree of metal−metal coupling, and the $\Delta\nu_{1/2}$ values for the most weakly coupled pentaammine complexes, ca. 4000 cm^{-1}, are consistent with other Class II complexes.[21] We regard the majority of the complexes of this study as strongly coupled Class II systems with some showing borderline Class III behavior as will be discussed later.

For the CNS model, the metal−ligand coupling element H_{LM} for a given Ru(III)−NCN bond was determined from the LMCT oscillator strength of the [III,III] complex. Equation 1 cannot be used as given, because the parameters therein assume Gaussian bands, and the LMCT band shapes are non-Gaussian. Calculation of the coupling elements were effected directly from experimental oscillator strengths determined for each spectrum by modeling the band envelope with multiple Gaussian bands.[20b] The oscillator strengths of the fitting bands were individually determined according to

$$f = (4.61 \times 10^{-9})(\epsilon_{max}\Delta\nu_{1/2}) \qquad (12)$$

and the total oscillator strength taken as the sum of the contributions of the various fitting bands. No significance was attributed to the number or nature of the fitting bands. Because the total LMCT oscillator strength arises from two equivalent Ru(III)−NCN chromophores in the [III, III] complex, f' is the normalized oscillator strength per Ru−NCN chromophore, and is thus half the total oscillator strength for the observed LMCT band. Equation 13 was used in place of eq 1 to solve for the various H_{LM}.

Table 10. Hush Model Predicted Bandwidths and Metal−Metal Coupling Elements, CNS Model Metal−Ligand and Metal−Metal Coupling Elements, and Reduced Metal−Ligand Energy Differences for the Complexes $[\{mer\text{-}Ru(NH_3)_3(bpy)\}_2(\mu\text{-L})]^{3+}$ as a Function of Ligand and Solvent. Experimental Estimates of IT Bandwidths and Free Energies of Resonance Exchange are Provided for Comparison[a]

		exptl	Hush model		CNS model			exptl
L	solvent	$\Delta\nu_{1/2}$	$\Delta\nu_{1/2}$[b]	H_{ad}	H_{LM}[c]	ΔE_{LM}[d]	$H_{MM'}$[e]	$\Delta G_r'$[f]
Me_2dicyd^{2-}	AN	1760	4290	640	2920	2650	3220	
$dicyd^{2-}$	AN	1700	4180	770	2950	2410	3610	
$dicyd^{2-}$	DMSO	2340	3930	940	2650	2460	2850	
Cl_2dicyd^{2-}	NM	2290	4020	980	2830	2560	3130	
Cl_2dicyd^{2-}	AN	2440	4000	1090	2720	2460	3010	1160
Cl_2dicyd^{2-}	AC	2140	3960	1060	2690	2500	2890	
Cl_2dicyd^{2-}	DMSO	3440	3840	1180	2260	3120	1640	650

[a] All data in cm^{-1}. [b] Hush predicted bandwidths calculated according to $\Delta\nu_{1/2}(\text{Hush}) = (2910\nu_{max})^{1/2}$ cm^{-1}. [c] Calculated according to eqs 12 and 13. [d] Calculated according to eq 4. [e] Calculated according to eq 3. [f] $\Delta G_r' = 0.5(\Delta G_r)$ in Table 7.

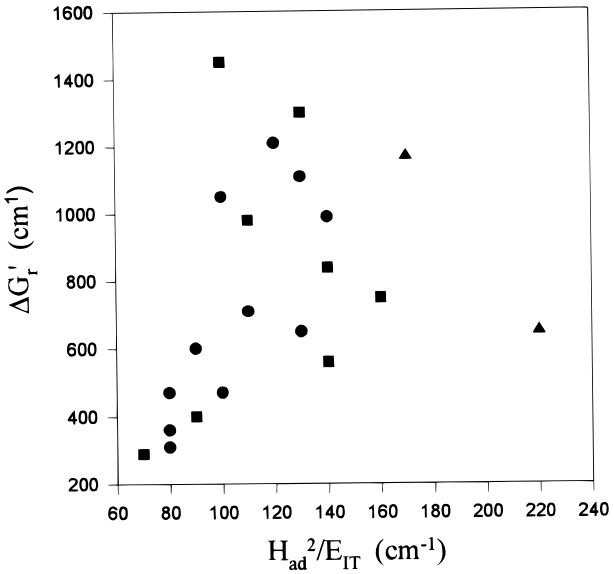

Figure 5. "Shotgun" plot of metal−metal coupling elements $\Delta G_r'$ vs H_{ad}^2/E_{IT} for the pentaammine (■), tetraammine (●), and triammine (▲) complexes. The data may be found in Tables 1−3 and 8−10.

$$H_{LM} = \frac{3.03 \times 10^2}{r}(E_{LMCT} \cdot f')^{1/2} \quad (13)$$

where $r = 6.5$ Å, which is the distance between Ru(III) and the center of the dicyd^{2-} bridging ligand.

In accordance with the hole-transfer superexchange mechanism shown in Figure 1, the reduced energy gap, ΔE_{LM}, should be smallest for the highest energy π-HOMO and for the most stable metal πd-orbitals (in the least electron donating solvents). For example, the results for the pentaammines, in Table 8, reflect this expectation exactly, with ΔE_{LM} being lowest when L = Me_2dicyd^{2-} and highest when L = Cl_4dicyd^{2-} for a given solvent and with ΔE_{LM} being lowest in nitromethane and highest in DMSO for a given complex. As the energy difference between the ruthenium πd-orbitals and the ligand π-HOMO is decreased, their interaction is expected to increase. Thus H_{LM} for each complex is highest in nitromethane and lowest in DMSO, and in acetonitrile it is highest when L = Me_2dicyd^{2-} and lowest when L = Cl_4dicyd^{2-}. The CNS model derived values of H_{LM} are in agreement with qualitative expectations of Ru(III)−cyanamide π interactions. It remains to be seen if metal−metal coupling can be adequately predicted.

The success of the CNS model in predicting metal−metal coupling for the complexes of this study is shown by the good correlation between $H_{MM'}^2/E_{IT}$ and $\Delta G_r'$ for the pentaammine, tetraammine, and triammine complexes in Figure 6. The plot in Figure 6 should be contrasted to the lack of correlation between H_{ad}^2/E_{IT} and $\Delta G_r'$ in Figure 5. While it may be tempting to draw a linear correlation for the plot in Figure 6, we believe that the slight curvature in data point distribution is real and a consequence of the inherent overestimation of $\Delta G_r'$ by $H_{MM'}^2/E_{IT}$. This is because as $H_{MM'}$ approaches E_{IT}, $\Delta G_r'$ approaches a limiting value of $H_{MM'}$ instead of the proper value of $H_{MM'} - \Delta G_{th}$, as shown in Figure 2B. In addition, a comparison between pentaammine and tetraammine data in Figure 6 shows a significant spread in $\Delta G_r'$ for complexes possessing roughly the same $H_{MM'}^2/E_{IT}$ value. This suggests that very small changes in electronic structure can dramatically affect the degree of metal−metal coupling. In Figure 6, $\Delta G_r'$ is approximately 200 cm^{-1} when $H_{MM'}^2/E_{IT} = 0$. This may result from underestimated values of ΔG_{ne} in Table 4 that were used to calculate ΔG_r. We used the value of ΔG_{ne} in water to estimate ΔG_{ne} in aprotic solvents. However, water has acceptor as well as donor properties and this may play a role in reducing ΔG_c. Indeed, it has been shown that antiferromagnetic coupling of the pentaammine complexes in aprotic solvents is significantly greater and follows a different trend when compared to aqueous solution data.[24]

For many of the tetraammine and most of the triammine complexes it is not possible to calculate ΔG_r with confidence because of the inability to determine ΔG_{ex}. This is unfortunate because these complexes represent the strongest coupling cases and their properties could be used to test the limits of the CNS model. We can use the Creutz−Taube ion [{Ru(NH_3)$_5$}$_2$-(μ-pyrazine)]$^{5+}$, where $\Delta G_c = 3150$ cm^{-1} in aqueous solution,[25] as a benchmark for a Class III assignment to the complexes of this study. In Tables 6 and 7, there are four complexes in nitromethane or acetonitrile solution that possess $\Delta G_c > 3000$ cm^{-1} and for these, eq 10 should apply. Estimates of ΔG_{th} in addition to ΔG_{ex} are required before the CNS model can be tested for these Class III systems.

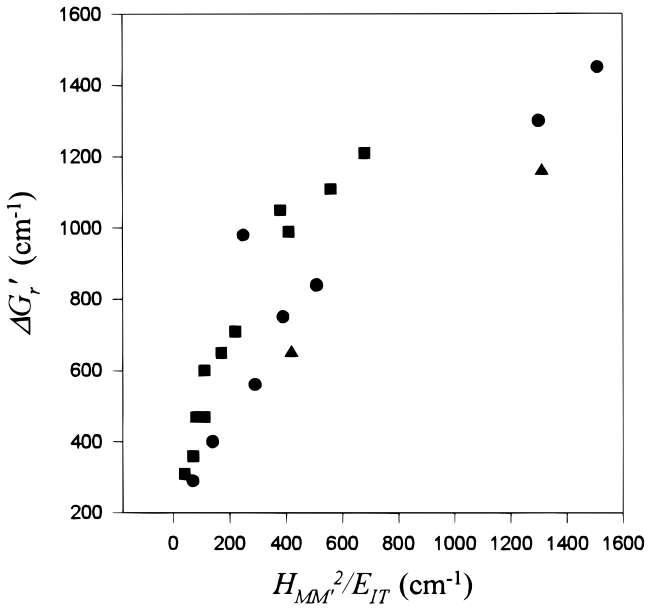

Figure 6. Plot of $\Delta G_r'$ vs $H_{MM'}^2/E_{IT}$ for the pentaammine (■), tetraammine (●), and triammine (▲) complexes. The data may be found in Tables 1−3 and 8−10.

Conclusion

We have shown that the CNS model successfully predicts the magnitude of hole-transfer superexchange for the Class II mixed-valence complexes of this study. Its usefulness to researchers lies in its simplicity of application, relying as it does on easily obtained spectral parameters and the realization that metal−ligand and metal−metal coupling elements are related to charge-transfer band oscillator strengths.

Acknowledgment. Dedicated to Dr. Keith U. Ingold, NRC Canada. We are grateful to the Natural Sciences and Engineering Research Council of Canada for financial support. We also thank Johnson-Matthey Ltd. for the loan of ruthenium trichloride hydrate.

JA982673B

(25) Creutz, C.; Taube, H. *J. Am. Chem. Soc.* **1973**, *95*, 1086.